Global nuclear structure effects of the tensor interaction

M. Zalewski,[1] P. Olbratowski,[1] M. Rafalski,[1] W. Satuła,[1,2] T. R. Werner,[1] and R. A. Wyss[2]
[1]*Institute of Theoretical Physics, University of Warsaw, Hoża 69, PL-00681 Warsaw, Poland*
[2]*KTH Royal Institute of Technology, AlbaNova University Center, S-10691 Stockholm, Sweden*
(Received 31 August 2009; published 8 December 2009)

A direct fit of the isoscalar spin-orbit (SO) and both isoscalar and isovector tensor coupling constants to the $f_{5/2}$-$f_{7/2}$ SO splittings in ^{40}Ca, ^{56}Ni, and ^{48}Ca nuclei requires a drastic reduction of the isoscalar SO strength and strong attractive tensor coupling constants. The aim of this work is to address further consequences of these strong attractive tensor and weak SO fields on binding energies, nuclear deformability, and high-spin states. In particular, the contribution to the nuclear binding energy from the tensor field shows a generic *magic structure* with *tensorial magic numbers* $N(Z) = 14$, 32, 56, or 90, corresponding to the maximum spin asymmetries in $1d_{5/2}$, $1f_{7/2} \oplus 2p_{3/2}$, $1g_{9/2} \oplus 2d_{5/2}$, and $1h_{11/2} \oplus 2f_{7/2}$ single-particle configurations, respectively, and that these numbers are smeared out by pairing correlations and deformation effects. The consequences of strong attractive tensor fields and weak SO interaction for nuclear stability at the drip lines are also examined, particularly those close to the *tensorial doubly magic* nuclei. The possibility of an entirely new tensor-force-driven deformation effect is discussed.

DOI: 10.1103/PhysRevC.80.064307 PACS number(s): 21.30.Fe, 21.10.Pc, 21.60.Cs, 21.60.Jz

I. INTRODUCTION

The primary goal of energy-density-functional (EDF) methods is to describe the ground-state energies of fermion systems (i.e., masses of nuclei in nuclear physics applications). The existence of a universal functional describing *exactly* the masses of odd, odd-odd, and even-even nuclei is warranted by the Hohenberg-Kohn [1] and Kohn-Sham [2] theorems. These theorems, however, provide no universal rules for the construction of such a functional. The complexity of the functional and our lack of knowledge with respect to the in-medium strong interaction that governs the structure of finite nuclei make the situation even more difficult. It does not permit the determination for any *ab initio* constraints of the nuclear EDF except for dilute neutron systems [3]. It forces the use of effective functionals with coupling constants fitted directly to the data. Hence, a proper selection of empirical data to be used in the process of constraining parameters of the functional becomes, irrespective of the form of the functional, the key issue for overall good performance of the nuclear density-functional theory (DFT) [4].

The typical strategy used to construct the nuclear EDF is to start with either the finite-range Gogny [5] or the zero-range Skyrme [6] effective interaction and to construct a nonlocal or local functional, respectively, by averaging the interaction within the Hartree-Fock (HF) method. The data sets used to adjust the free parameters of the theory are dominated by bulk nuclear matter data and by nuclear binding energies of selected doubly magic nuclei; much less attention is paid to the single-particle energies (SPEs).

The major reason is the effective mass scaling of the single-particle (SP)-level density, g, in the vicinity of the Fermi energy ε_F. In homogeneous nuclear matter the SP-level density scales according to the following simple rule: $g(\varepsilon_F) \rightarrow \frac{m}{m^*} g(\varepsilon_F)$. In finite nuclei the situation is slightly more intricate, mostly because of the $\mathbf{r}$-dependence of $m^*(\mathbf{r})$. Several authors [7–9] analyzed SP-level density scaling and argued that the physical density of SP levels around the Fermi energy can be restored only after the inclusion of particle-vibration coupling [i.e., by going beyond the mean field (MF)]. This viewpoint is difficult to reconcile with the effective EDF theories. Indeed, these theories should warrant a proper value of the effective mass through the fit to the empirical data and should readjust other coupling constants to this value of m^*. This approach should lead to fairly m^*-independent predictions, provided that the (spherical) SPEs are calculated from the differences between the binding energies in even-even doubly magic cores and the lowest SP states in odd-A single-particle/hole neighbors. Within the EDF approach, the mean-field or, more precisely, Kohn-Sham SP energies computed in an even-even doubly magic core serve only as auxiliary quantities.

A new strategy for fitting the spin-orbit (SO) and tensor parts of the nuclear EDF was recently suggested by our group [10]. Instead of performing large-scale fits to binding energies, a simple and intuitive three-step procedure was proposed that can be used to fit the isoscalar strength of the SO interaction as well as the isoscalar and isovector strengths of the tensor interaction. The entire idea is based on the observation that the $f_{7/2}$-$f_{5/2}$ SO splittings in spin-saturated isoscalar ^{40}Ca, spin-unsaturated isoscalar ^{56}Ni, and spin-unsaturated isovector ^{48}Ca form distinct patterns that can be neither understood nor reproduced based solely on the conventional SO interaction. Following the general philosophy of the nuclear DFT, we compute the $f_{7/2}$-$f_{5/2}$ SO splittings from the differences between the binding energies of these doubly magic cores and their odd-A neighbors. However, the same functional is used to calculate both the ground-state energies, which is well justified, and the low-lying SP excitations in the odd-A neighbors. The reasonability of the latter assumption remains to be studied.

The procedure reveals the need for a sizable reduction (from ∼20% up to ∼35% depending on the parametrization and,

in particular, on the value of m^*) of the SO strength and, at the same time, for much stronger tensor fields compared to the commonly used values. The new parametrization systematically improves the performance of the functional with respect to SP properties like the SO splittings or the magic gaps but it deteriorates the binding energies [10]. The aim of the present work is to address further the consequences of a strong attractive tensor and weak SO fields on binding energies, time-even and time-odd polarization effects, and nuclear deformability. The paper is organized as follows. Sec. II briefly presents the theoretical background of our model. In Sec. III, it is shown that the contribution to the binding energy due to the tensor interaction forms a generic pattern closely resembling that of the shell correction with the tensorial magic numbers shifted up compared to the standard magic numbers toward $N(Z) = 14, 32, 56$, or 90. The tensorial magic numbers reflect the maximum spin-asymmetry in $1d_{5/2}$, $1f_{7/2} \oplus 2p_{3/2}$, $1g_{9/2} \oplus 2d_{5/2}$, and $1h_{11/2} \oplus 2f_{7/2}$ configurations, respectively, in the extreme SP scenario for a spherical shape. The tensorial magic structure is smeared out by configuration mixing caused by pairing and deformation effects. In Sec. IV it is demonstrated that one can construct an EDF capable of reproducing reasonably well both the SO splittings and the binding energies of the doubly magic spherical nuclei. In Sec. V the influence of strong tensor fields on time-even and time-odd polarization effects in the $f_{7/2}$-$f_{5/2}$ SO splittings is dicussed. In Sec. VI, deformation properties of the new functionals and a possible novel mechanism related to the onset of nuclear deformation in the presence of strong attractive tensor fields are discussed. The paper is concluded in Sec. VII. This analysis complements preliminary results communicated in two earlier conference publications [11,12].

II. THEORY: FROM TWO-BODY SPIN-ORBIT AND TENSOR INTERACTIONS TO ENERGY-DENSITY FUNCTIONALS AND MEAN FIELDS

In our study we explore the local EDF $\mathcal{H}(\mathbf{r})$. It is the sum of the kinetic energy and the isoscalar ($t = 0$) and isovector ($t = 1$) potential energy terms:

$$\mathcal{H}(\mathbf{r}) = \frac{\hbar^2}{2m}\tau_0 + \sum_{t=0,1}[\mathcal{H}_t(\mathbf{r})^{\text{even}} + \mathcal{H}_t(\mathbf{r})^{\text{odd}}], \tag{1}$$

which are conventionally decomposed into parts built of bilinear forms of either only time-even or only time-odd densities, currents, and their derivatives:

$$\begin{aligned}\mathcal{H}_t^{\text{even}} &= C_t^{\rho}[\rho_0]\rho_t^2 + C_t^{\Delta\rho}\rho_t\Delta\rho_t \\ &\quad + C_t^{\tau}\rho_t\tau_t + C_t^{J}\mathbb{J}_t^2 + C_t^{\nabla J}\rho_t\nabla\cdot\mathbf{J}_t,\end{aligned} \tag{2}$$

$$\begin{aligned}\mathcal{H}_t^{\text{odd}} &= C_t^{s}[\rho_0]\mathbf{s}_t^2 + C_t^{\Delta s}\mathbf{s}_t\cdot\Delta\mathbf{s}_t \\ &\quad + C_t^{T}\mathbf{s}_t\cdot\mathbf{T}_t + C_t^{j}\mathbf{j}_t^2 + C_t^{\nabla j}\mathbf{s}_t\cdot(\nabla\times\mathbf{j}_t).\end{aligned} \tag{3}$$

For the time-even (ρ_t, τ_t, and $\mathbb{J}_t$) and time-odd ($\mathbf{s}_t$, $\mathbf{T}_t$, and $\mathbf{j}_t$) local densities, we follow the convention introduced in Ref. [13] (see also Refs. [14] and [15] and references cited therein).

The present study focuses on the spin-orbit and tensor parts of the EDF:

$$\mathcal{H}^{T} = C_0^{J}\mathbb{J}_0^2 + C_1^{J}\mathbb{J}_1^2, \tag{4}$$

$$\mathcal{H}^{\text{SO}} = C_0^{\nabla J}\rho_0\nabla\cdot\mathbf{J}_0 + C_1^{\nabla J}\rho_1\nabla\cdot\mathbf{J}_1. \tag{5}$$

These two parts of the EDF are strongly tied together through their mutual and unique contributions to the one-body spin-orbit potential. This relation can be best visualized by decomposing the spin-current tensor density $\mathbb{J}_{\mu\nu}$ into scalar $J^{(0)}$, vector J_μ, and symmetric-tensor densities $J^{(2)}_{\mu\nu}$,

$$\mathbb{J}_{\mu\nu} = \frac{1}{3}J^{(0)}\delta_{\mu\nu} + \frac{1}{2}\varepsilon_{\mu\nu\eta}J_\eta + J^{(2)}_{\mu\nu}, \tag{6}$$

$$\mathbb{J}^2 \equiv \sum_{\mu\nu}\mathbb{J}^2_{\mu\nu} = \frac{1}{3}(J^{(0)})^2 + \frac{1}{2}\mathbf{J}^2 + \sum_{\mu\nu}\left(J^{(2)}_{\mu\nu}\right)^2, \tag{7}$$

and going to the spherical-symmetry (SS) limit where the scalar $J^{(0)}$ and the symmetric-tensor densities $J^{(2)}_{\mu\nu}$ vanish identically. In this limit the spin-current tensor density,

$$\mathbb{J}_{\mu\nu} \xrightarrow{\text{SS limit}} \frac{1}{2}\varepsilon_{\mu\nu\eta}J_\eta \quad \text{and} \quad \mathbb{J}^2 \xrightarrow{\text{SS limit}} \frac{1}{2}\mathbf{J}^2, \tag{8}$$

reduces, therefore, to the spin-orbit vector density with a single radial component, $\mathbf{J}_t = \frac{\mathbf{r}}{r}J_t(r)$. The variation of the tensor and SO parts of the EDF over the radial SO densities $J(r)$ gives the spherical isoscalar ($t = 0$) and isovector ($t = 1$) SO MFs,

$$W_t^{\text{SO}} = \frac{1}{2r}\left[C_t^{J}J_t(r) - C_t^{\nabla J}\frac{d\rho_t}{dr}\right]\mathbf{L}\cdot\mathbf{S}, \tag{9}$$

which can be easily translated into the neutron ($q = n$) and proton ($q = p$) SO MFs,

$$\begin{aligned}W_q^{\text{SO}} = \frac{1}{4r}\Big[&\left(C_0^{J} - C_1^{J}\right)J_0(r) + 2C_1^{J}J_q(r) \\ &- \left(C_0^{\nabla J} - C_1^{\nabla J}\right)\frac{d\rho_0}{dr} - 2C_1^{\nabla J}\frac{d\rho_q}{dr}\Big]\mathbf{L}\cdot\mathbf{S}.\end{aligned} \tag{10}$$

Next we perform calculations that assume neither spherical nor time-reversal symmetries. General expressions for the SO mean fields can be found in numerous references (see, e.g., Refs. [13,15]) and are not repeated here. Spherical formulas (9) and (10) are provided here because they are crucial for understanding the fitting strategy of the tensor and spin-orbit coupling constants, which rely on the $f_{7/2}$-$f_{5/2}$ SO splittings in spherical doubly magic ^{40}Ca, ^{56}Ni, and ^{48}Ca nuclei (see Ref. [10] and the discussion that follows).

The functional of the form of Eqs. (2) and (3) can be obtained by averaging the conventional Skyrme effective interaction, $v_{\text{Sk}}(\boldsymbol{r})$, within the Skyrme-Hartree-Fock (SHF) approximation [13]. In such an approach, 20 EDF coupling constants C_t are uniquely expressed by means of 10 auxiliary Skyrme-force parameters (see Ref. [14]). Hence, the SHF approximation superimposes relatively strong limitations on the EDF. However, it serves as a reasonable starting point for further studies. The EDF approach starting from the effective force also indicates possible ways of generalizing the nuclear EDF. In particular, an investigation of the tensor component requires the use of a generalized Skyrme force augmented by a local tensor interaction $v_T(\boldsymbol{r})$:

$$v(\boldsymbol{r}) = v_{\text{Sk}}(\boldsymbol{r}) + v_T(\boldsymbol{r}), \tag{11}$$

where

$$\begin{aligned} v_T(\mathbf{r}) = {} & \tfrac{1}{2}t_e\{[3(\boldsymbol{\sigma}_1\cdot\mathbf{k}')(\boldsymbol{\sigma}_2\cdot\mathbf{k}') - (\boldsymbol{\sigma}_1\cdot\boldsymbol{\sigma}_2)\mathbf{k}'^2]\delta(\mathbf{r}) \\ & + \delta(\mathbf{r})[3(\boldsymbol{\sigma}_1\cdot\mathbf{k})(\boldsymbol{\sigma}_2\cdot\mathbf{k}) - (\boldsymbol{\sigma}_1\cdot\boldsymbol{\sigma}_2)\mathbf{k}^2]\} \\ & + t_o[3(\boldsymbol{\sigma}_1\cdot\mathbf{k}')\delta(\mathbf{r})(\boldsymbol{\sigma}_2\cdot\mathbf{k}) - (\boldsymbol{\sigma}_1\cdot\boldsymbol{\sigma}_2)\mathbf{k}'\cdot\delta(\mathbf{r})\mathbf{k}] \end{aligned} \tag{12}$$

and, conventionally, $\mathbf{r} = \mathbf{r}_1 - \mathbf{r}_2$ and $\mathbf{k} = -\frac{i}{2}(\boldsymbol{\nabla}_1 - \boldsymbol{\nabla}_2)$ are relative coordinates and momentum and $\mathbf{k}'$ is the complex conjugation of $\mathbf{k}$ acting on the left-hand side. By averaging $v_T(\mathbf{r})$ within the HF approach, one obtains the following contribution to the time-even part of the EDF [15]:

$$\delta\mathcal{H}_t^{\text{even}} = \tfrac{5}{3}B_t^T\left[J_t^{(0)}\right]^2 - \tfrac{5}{4}B_t^T\mathbf{J}_t{}^2 + \tfrac{1}{2}B_t^T\sum_{\mu\nu}\left[J_{t,\mu\nu}^{(2)}\right]^2 \tag{13}$$

where

$$B_0^T = -\tfrac{1}{8}(t_e + 3t_o) \quad \text{and} \quad B_1^T = \tfrac{1}{8}(t_e - t_o). \tag{14}$$

Note that there are two independent contributions to the tensor part of the EDF. The Skyrme force contributes, through the exchange term, to the tensor part of the EDF in a uniform manner; that is, it depends on a unique coupling constant (4). In contrast, the tensor force contributes to the EDF in a nonuniform way. Hence, the tensor force generates a clear *theoretical* need to generalize the EDF (4) by using three independent coupling constants and multiplying each of the three terms appearing in Eq. (7):

$$\mathcal{H}_t^T \longrightarrow C_t^{J^{(0)}}\left[J_t^{(0)}\right]^2 + C_t^J\mathbf{J}_t{}^2 + C_t^{J^{(2)}}\sum_{\mu\nu}\left[J_{t,\mu\nu}^{(2)}\right]^2. \tag{15}$$

The effects of such an extension, in which the new coupling constants must be adjusted, can only be probed in deformed nuclei. Because conventional effective interactions and functionals are rather successful in describing nuclear deformation, no first-hand motivation exists for such a generalization. Hence, in the present study, we do not implement this possible extension of the EDF, and we use the unique tensor coupling constants C_t^J, as defined in Eq. (2).

The contribution to the time-odd part of the EDF coming from the tensor interaction is

$$\begin{aligned} \delta\mathcal{H}_t^{\text{odd}} = {} & B_t^T(\boldsymbol{s}_t\cdot\boldsymbol{T}_t - 3\boldsymbol{s}_t\cdot\boldsymbol{F}_t) \\ & + B_t^{\Delta s}[\boldsymbol{s}_t\cdot\Delta\boldsymbol{s}_t + 3(\boldsymbol{\nabla}\cdot\boldsymbol{s}_t)^2], \end{aligned} \tag{16}$$

where

$$B_0^{\Delta s} = \tfrac{3}{32}(t_e - t_o) \quad \text{and} \quad B_1^{\Delta s} = -\tfrac{1}{32}(3t_e + t_o). \tag{17}$$

New terms that appear in the time-odd part of the EDF, namely $\sim\boldsymbol{s}_t\cdot\boldsymbol{F}_t$ and $\sim(\boldsymbol{\nabla}\cdot\boldsymbol{s}_t)^2$, are not considered here mostly because of a lack of clear experimental indicators available to fit their strength. Extensive discussion linking the Skyrme forces to the tensor component in the EDF including, in particular, the definition of the density $\boldsymbol{F}_t$ can be found in Ref. [16] (see also Ref. [15]).

The starting point of our consideration is always the conventional Skyrme-force-inspired functional with coupling constants fixed at the values characteristic for either SkP [17], SLy4 [18], or SkO [19] Skyrme parametrization. The variants of the EDF with tensor and spin-orbit strengths modified along the prescription of Refs. [10,20] are marked by an additional subscript T: SkP_T, SLy4_T, and SkO_T. In the time-odd sector, two variants of the functional are tested with coupling constants fitted to the empirical values of the s-wave Landau parameters [21–23] $g_0 = 0.4$, $g_0' = 1.2$ and to the Gogny-force values of the p-wave Landau parameters [22,23] $g_1 = -0.19$, $g_1' = 0.62$:

$$g_0 = N_0\left(2C_0^s + 2C_0^T\beta\rho_0^{2/3}\right), \quad g_1 = -2N_0C_0^T\beta\rho_0^{2/3}, \tag{18}$$

$$g_0' = N_0\left(2C_1^s + 2C_1^T\beta\rho_0^{2/3}\right), \quad g_1' = -2N_0C_1^T\beta\rho_0^{2/3}, \tag{19}$$

where $\beta = (3\pi^2/2)^{2/3}$ and $N_0^{-1} = \pi^2\hbar^2/2m^\star k_F$ is an effective-mass-dependent normalization factor. In these variants of the EDF, we additionally assume density independence of coupling constant C_t^s, set the spin-surface term $C_t^{\Delta s} \equiv 0$, and assume gauge-invariant relations $C_t^j = -C_t^\tau$ and $C_t^{\nabla j} = C_t^{\nabla J}$. Concerning the time-odd tensor coupling constants, C_t^T, the following two possibilities are tested: (i) a broken gauge-symmetry scenario with C_t^T fitted to the Landau parameters and (ii) a gauge-invariant scenario with $C_t^T = -C_t^J$ determined using the time-even coupling constants C_t^J. The variants of the EDF with spin fields defined using the Landau parameters are labeled either by subscript L_S or subscript L_B for the gauge-invariant and the gauge-symmetry-violating functionals, respectively.

III. TOPOLOGY OF TENSOR CONTRIBUTION TO THE NUCLEAR BINDING ENERGY

The recent revival of interest in the tensor interaction was triggered by empirical discoveries of strong and systematic changes in the shell structure of neutron-rich oxygen [24], neon [25], sodium [26,27], magnesium [28], and titanium [29,30] nuclei, including a new shell gap opening at $N = 32$. These empirical discoveries were successfully interpreted within the nuclear shell model after the so-called monopole shifts were introduced. To account for the data, the monopole shifts are (i) attractive between $j_<^\nu$ and $j_<^\pi$ orbitals and (ii) repulsive between $j_<^\nu$ and $j_>^\pi$ orbitals where $j_\lessgtr = l \pm 1/2$. The physical origin of these monopole shifts was attributed to the tensor interaction [31–33]. Soon after successful shell-model calculations, the mechanism was confirmed to work within self-consistent MF calculations using finite-range Gogny force augmented by the finite-range tensor interaction (see Ref. [34]). It was shown in Ref. [34] that, apart from explaining the shell-structure evolution in light exotic nuclei, the tensor interaction could also account for empirical trends in the relative positions of the $1f_{5/2}$ and $1p_{3/2}$ levels in copper isotopes [35,36] or for the evolution of the single-particle $1h_{11/2}$-$1g_{7/2}$ level splittings versus N in antimony [37] isotopes.

The local tensor interaction within the SHF approximation was first studied in Ref. [38]. Based on the SPE analysis, the effective functional coupling constants C_t^J were evaluated to lie within the triangle [known as the Brink-Stancu-Flocard (BSF) triangle] marked schematically in Fig. 1. For strictly pragmatic reasons, like technical complexity and lack of firm experimental indicators further constraining the BSF

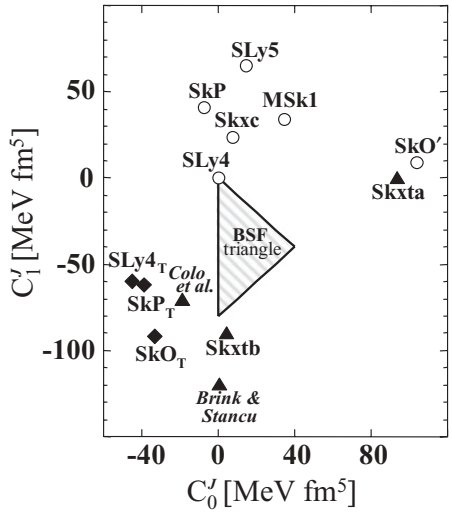

FIG. 1. The isovector, C_1^J, versus the isoscalar, C_0^J, tensor coupling constant. Open circles represent values of several popular parametrizations fitted predominantly to the binding energies of spherical nuclei. Black diamonds represent coupling constants deduced recently from direct fits to the SPE and the SP splittings [10]. Black triangles represent fits of Refs. [39–41]. The shaded area shows the so-called BSF triangle reflecting the range of the tensorial parameters deduced in a pioneering paper by Brink, Stancu, and Flocard [38].

estimate, in many Skyrme parametrizations (including SIII [42], SLy4 [18], SkM* [43], and SkO [19]), the tensor terms are simply disregarded by setting $C_t^J \equiv 0$. Moreover, the C_t^J coupling constants established predominantly through fits to bulk nuclear data seem to contradict the BSF estimates. Indeed, the isoscalar-tensor coupling constants of such popular forces as SLy5 [18], SkP [17], or Skxc [44] are relatively weak whereas their isovector coupling constants are positive. These coupling constants lie outside the BSF triangle, as shown in Fig. 1.

However, direct fits to the SP-level splittings [10,39,41] clearly reveal that drastic changes in the commonly accepted tensor coupling constants are needed to account for the SP data. This is visualized in Fig. 1, where the new parametrizations are marked by black triangles and black diamonds, respectively. The fact that new values of C_t^J are still slightly scattered is a consequence of both different fitting strategies and different starting-point parametrizations used by different groups.

Our strategy of fitting the coupling constants of the nuclear EDF (see Ref. [10]) differs from the strategies applied by other groups. Unlike other groups, we simultaneously fit the isoscalar spin-orbit, $C_0^{\nabla J}$, as well as the isoscalar and the isovector tensor coupling constants, C_0^J and C_1^J, respectively, using a simple three-step method. The entire idea of this procedure is based on the observation that the empirical $1f_{7/2}$-$1f_{5/2}$ SO splittings in ^{40}Ca, ^{56}Ni, and ^{48}Ca form a distinct pattern that cannot be reproduced solely by using the conventional SO interaction. The readjustment of the coupling constants proceeds as follows: (i) $C_0^{\nabla J}$ is established in the isoscalar spin-saturated nucleus ^{40}Ca, (ii) the C_0^J coupling constant is readjusted in spin-unsaturated isoscalar nucleus ^{56}Ni, and, finally, (iii) the C_1^J coupling constant is readjusted to the spin-unsaturated isovector nucleus ^{48}Ca.

Our results (see Refs. [10–12,20]) show that drastic changes in the isoscalar SO strength and the tensor coupling constants are required compared to commonly accepted values. In turn, one obtains systematic improvements for such SP properties as SO splittings and magic gap energies. It is also interesting to note that the isoscalar SO and the isoscalar tensor coupling constants resulting from such a fit are to large extent independent of the parametrization and equal to $C_0^{\nabla J} \approx -60 \pm 10$ MeV fm^5 and $C_0^J \approx -40 \pm 10$ MeV fm^5, respectively. The uncertainties are rough estimates that reflect the sensitivity of the method. The isovector tensor coupling constant, C_1^J, is less certain. It depends on the actual ratio of the SO coupling constants, $C_0^{\nabla J}/C_1^{\nabla J}$, which, in the adjustment process, was kept fixed at its Skyrme-force value because of a lack of empirical data for ^{48}Ni, which does not allow for firm independent readjustment of the fourth coupling constant, $C_1^{\nabla J}$.

The influence of the tensor interaction on nuclear SPE and SP-level splittings has been analyzed by many authors. It was shown that the tensor interaction leaves unique and robust fingerprints when the SPE and SP-level splittings are studied along isotopic or isotonic chains. It also appears that the contribution to the binding energy coming from the tensor interaction, $\delta B_T(N, Z)$, shows several highly interesting and robust topological features. In particular, the contribution $\delta B_T(N, Z)$ shows a generic pattern closely resembling that of a shell correction. The tensorial magic numbers at $N(Z) = 14$, 32, 56, or 90 correspond to the maximum spin-asymmetries in $1d_{5/2}$, $1f_{7/2} \oplus 2p_{3/2}$, $1g_{9/2} \oplus 2d_{5/2}$, and $1h_{11/2} \oplus 2f_{7/2}$ SP configurations, respectively, in the extreme SP scenario at spherical shape. The robustness (i.e., the model independence of the tensorial magic pattern) results from the rather unambiguously established order of SP levels, which is relatively well reproduced by state-of-the-art nuclear MF models, particularly for light- and medium-mass nuclei. Note that the tensorial magic numbers are only slightly shifted compared to classic magic numbers at $N(Z) = 8$, 20, 28, 50, and 82.

The tensorial magic pattern is clearly visible in Fig. 2. Figures 2(a)–2(c) show the contribution to the binding energy coming from (a) the isovector part of the tensor term, $\delta E_1^T = C_1^J \int d^3\boldsymbol{r}\mathbb{J}_1^2(\boldsymbol{r})$; (b) the isoscalar part of the tensor term, $\delta E_0^T = C_0^J \int d^3\boldsymbol{r}\mathbb{J}_0^2(\boldsymbol{r})$; and (c) the total tensor contributions to the EDF. These calculations were performed using the spherical Hartree-Fock-Bogolyubov (HFB) code HFBRAD [45] with the SLy4$_T$ functional of Ref. [10] in the particle-hole channel and the volume-δ interaction in the pairing channel. This part of Fig. 2 shows several interesting features:

(i) Additional smearing of the SP tensorial magic structure occurs due to configuration mixing caused by nuclear pairing. In light- and medium-mass nuclei, substantial tensor contributions are located in relatively broad regions centered around the SP tensorial magic

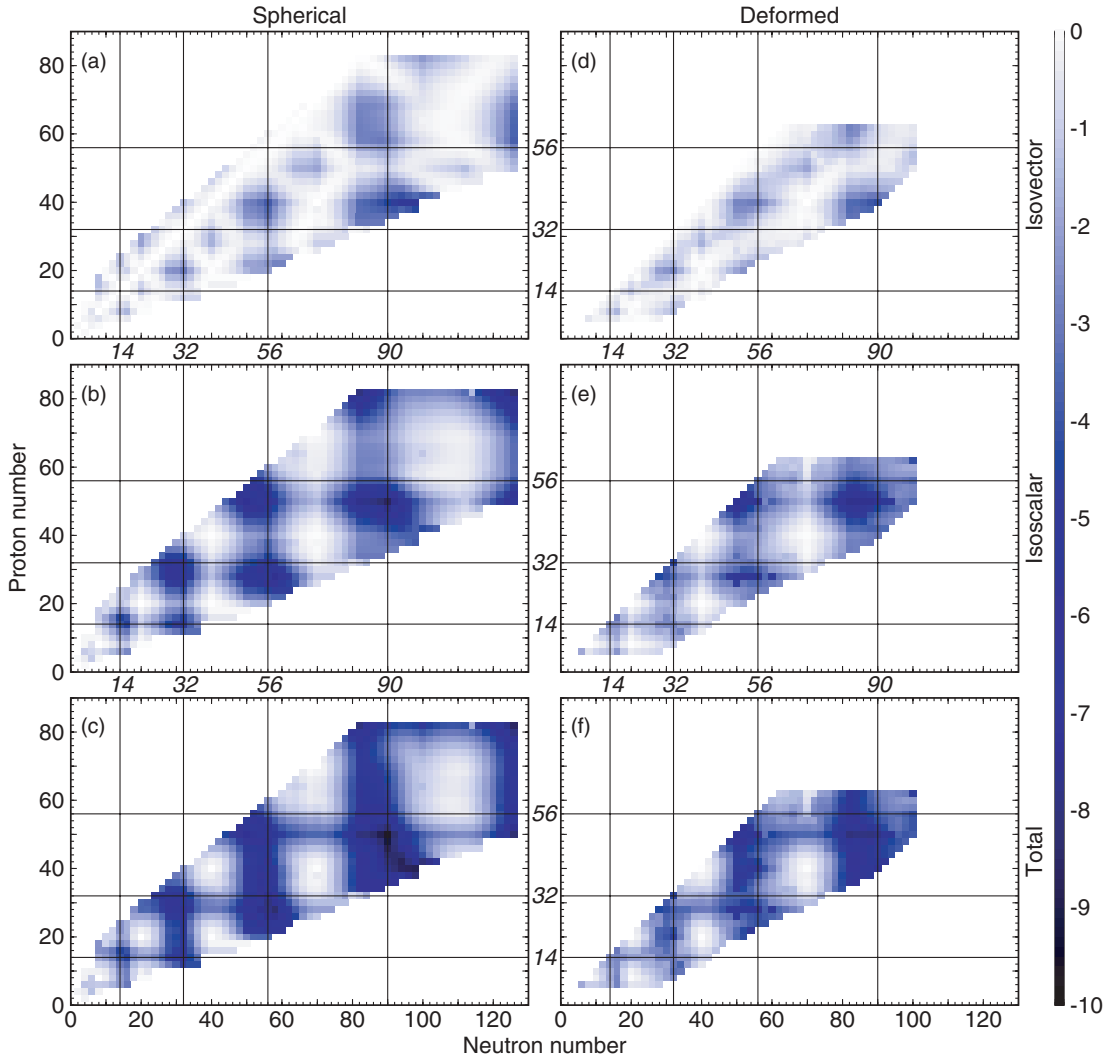

FIG. 2. (Color online) The isovector (top), the isoscalar (middle), and the total (bottom) tensor contribution to the nuclear binding energy obtained from spherical (left) and deformed (right) HFB calculations. Both sets of calculations were done using the SLy4$_T$ interaction in the particle-hole channel and the volume-δ interaction in the particle-particle channel. Vertical and horizontal lines indicate single-particle tensorial magic numbers at spherical shape. See text for further details.

numbers. In heavier nuclei, where pairing effects are relatively stronger due to the larger density of SP levels, the erosion of the SP tensorial magic structure is stronger. The maximum of the tensor contribution is shifted away from the SP magic numbers. The details, however, are strongly model dependent, mostly because of large uncertainties in the positions of the SP levels in heavier nuclei. Indeed, problems persist in using Skyrme models to reproduce absolute positions of the experimental SPE as shown recently in Ref. [46].

(ii) The contribution from the isovector part of the tensor interaction is much weaker than the isoscalar contribution. This conclusion depends on the tensorial coupling constants.

(iii) The isoscalar tensor interaction creates *oscillatory* effects in nuclear masses that depend on the degree of spin-unsaturation in a given nucleus. This additional nonuniform N and Z dependence, in particular, may obscure conclusions deduced from the widely used binding-energy indicators technique.

The second major source of configuration mixing comes from the spontaneous breaking of spherical symmetry inherent in the MF method. The influence of nuclear deformation on the topology of the tensor contributions to the binding energy is illustrated in Figs. 2(d)–2(f). The calculations presented in the figure were performed for even-even nuclei with $N \geqslant Z$ and the range $6 \leqslant Z \leqslant 64$ using the HFODD code [47]. The same SLy4$_T$ interaction of Ref. [10] was used in the particle-hole channel and volume-δ interaction in the particle-particle channel. It is clearly visible that the effect of deformation does not change the topology of the tensor energy contribution; it strongly reduces its magnitude. One should stress though that the quantitative estimate of the deformation effect is uncertain. The magnitude of the deformation is extremely sensitive to

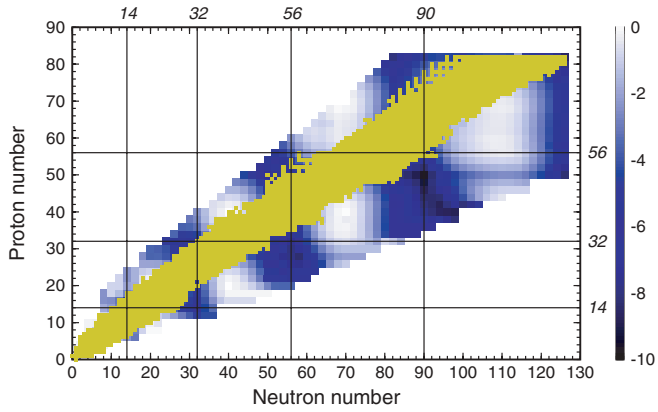

FIG. 3. (Color online) Tensor contribution to the total binding energy obtained from spherical HFB calculations. The map is overlaid with the map of known nuclei (according to Ref. [48]). The figure illustrates these regions where strong tensor effects may be expected in neutron- and proton-rich nuclei.

the balance between SO and tensor strengths. This effect is discussed in detail in Sec. V.

Figure 3 shows again the total contribution to the binding energy calculated using the spherical HFB model. The map is overlaid with the map of known nuclei, according to Ref. [48]. The aim of the figure is to illustrate mass regions where enhanced tensor effects, and in turn perhaps new physics, may be expected on the neutron- and proton-rich sides. On the neutron-rich side, the regions of interest (i.e., those which are or can be accessible experimentally in the nearest future) include $Z \approx 14$ and $N \approx 32$, $Z \approx 32$ and $N \approx 56$, and $Z \approx 56$ and $N \approx 90$. In particular, recent measurements of exotic ${}^{40}_{12}\mathrm{Mg}_{28}$ and ${}^{42}_{13}\mathrm{Al}_{29}$ by Bauman *et al.* [49] (see also the discussion in Ref. [50]) approach closely the first of the aforementioned mass regions. However, whether or not extra binding due to the strong attractive tensor interaction gives rise to stabilization of these nuclei and nuclei around them remains to be studied. MF calculations using conventional Skyrme forces predict these nuclei to be bound [51].

IV. ENERGY-DENSITY FUNCTIONAL FITTED TO SINGLE-PARTICLE SPIN-ORBIT SPLITTINGS AND TO THE TOTAL BINDING ENERGIES OF SPHERICAL NUCLEI

The topology of the tensor contribution to the total binding energy is, as discussed earlier, a generic feature related to shell structure and the degree of spin-saturation. However, the quantitative features, including the total magnitude and the isovector-to-isoscalar ratio of the tensor contributions, depend on the actual values of the tensorial coupling constants. The two strategies of fitting effective forces—namely the conventional one based on the large-scale fit to the binding energies and the one based on the fit of C_t^J and $C_t^{\nabla J}$ coupling constants directly to the SO splittings—seem to yield contradicting results. This result is clearly visible in Fig. 1, where the ranges of the C_t^J strengths deduced using these two methods simply exclude each other.

A direct fit to the SO splittings leads to drastic changes in the isoscalar SO strength and the tensor coupling constants compared to commonly accepted values. In particular, the pronounced reduction of the SO strength, which varies from 20% for large effective mass forces, m^*, to even 35% for low forces ($m^* \approx 0.7$), jeopardizes the agreement with observed binding energies. This effect cannot be solely compensated by strong attractive tensor fields. Hence, further readjustments of the other coupling constants of the EDF are necessary to ensure good performance for masses.

In Ref. [10] it was demonstrated that a considerable improvement in the quality of mass fits can be achieved be relatively small readjustments of the EDF coupling constants. For the purpose of this work, we performed similar calculations using a multidimensional minimization technique but starting from the SkP_T force. In both cases, tiny modifications (of the order of a fraction of a percent) in the coupling constants clearly improve the quality of the mass fit compared to the $\mathrm{SLy4}_T$ and SkO_T forces but still do not provide the quality of the original SLy4 and SkO parametrizations.

Inherent to the multidimensional minimization technique is a merit function as a subject of minimization. In our calculations, the merit function is constructed out of relative deviations from measured masses of selected spherical doubly magic nuclei. It appears that the merit function in the multidimensional space spanned by the EDF coupling constants varying in the minimization process is very steep for some specific directions and extremely flat in others. This finding implies that the entire minimization problem is not well defined. We visualize this by taking the SkO parametrization as a starting point.

By reducing the SO strength by 15%, corresponding to $C_0^J \approx -65.6$ MeV fm^5 and $C_1^J \approx 84.5$ MeV fm^5 and taking $C_0^J = -44.1$ MeV fm^5 and $C_1^J = -91.6$ MeV fm^5, we create a modified version of the SkO_T parametrization of Ref. [10]. This parametrization, dubbed $\mathrm{SkO}_{T'}$, has a slightly stronger SO term and more attractive tensor fields compared to the SkO_T functional. These changes aim to improve the mass performance of the SkO_T functional. Direct calculations show (see Fig. 4) that the $\mathrm{SkO}_{T'}$ functional reproduces masses at a level of accuracy similar to one of the most popular SLy forces. The calculations illustrated in Fig. 4 were performed using the HFODD code with 20 spherical shells. For this study we had to use the HFODD code because the spherical HFBRAD code has no two-body center-of-mass correction implemented.

The performance of the $\mathrm{SkO}_{T'}$ force can be further improved in many different ways. One example, dubbed $\mathrm{SkO}_{T''}$, is illustrated in Fig. 4. This force was obtained by readjusting isoscalar and isovector central fields in the following way: $C_0^\rho \to 1.00015 C_0^\rho$ and $C_1^\rho \to 0.99 C_1^\rho$. As a result, the standard deviation drops from $\sigma(\mathrm{SkO}_{T'}) \approx 1.663$ MeV to $\sigma(\mathrm{SkO}_{T''}) \approx 1.475$ MeV where, for comparison, $\sigma(\mathrm{SLy4}) \approx 1.879$ MeV. Similar improvements can be made, by readjusting the density-dependent term, for example.

A reasonable performance of the $\mathrm{SkO}_{T'}$ or $\mathrm{SkO}_{T''}$ functionals with respect to the binding energies of spherical doubly magic nuclei is of great interest. It may help to resolve the conflict between the tensor and SO coupling constants

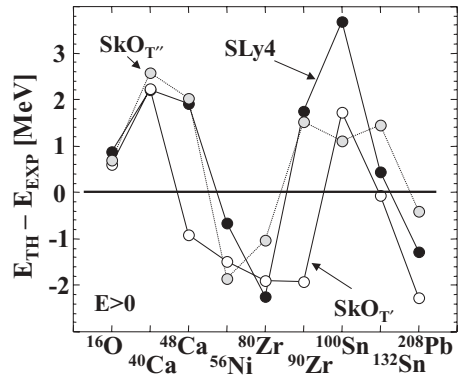

FIG. 4. Differences between theoretical and experimental binding energies in spherical doubly magic nuclei and in ^{80}Zr. The calculations have been done using the SkO$_{T'}$ (white dots) and SkO$_{T''}$ (gray dots) functionals. The conventional SLy4 Skyrme-force result (black dots) is also shown for the sake of comparison.

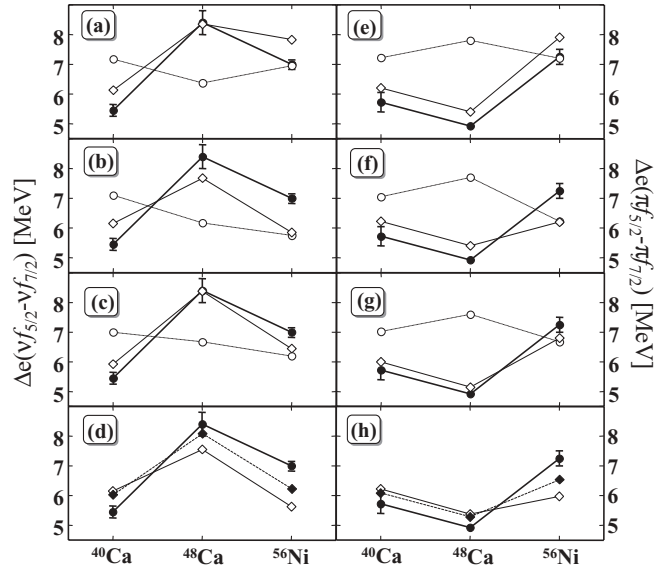

FIG. 5. SO splittings between (a)–(d) the neutron $\nu 1f_{5/2}$ and $\nu 1f_{7/2}$ and (e)–(h) the proton $\pi 1f_{5/2}$ and $\pi 1f_{7/2}$ (right part) orbitals in ^{40}Ca, ^{48}Ca, and ^{56}Ni nuclei. Filled or open circles mark empirical and theoretical splittings calculated using the conventional SkO force, respectively. Open and filled diamonds indicate calculations performed using the SkO$_{T'}$ functional. Panels (a) and (e) show bare, unpolarized SO splittings deduced directly from the SP spectra calculated in the doubly magic ^{40}Ca, ^{48}Ca, and ^{56}Ni nuclei. Parts (b) and (f) include only the time-even (mass and deformation) polarization effect. Panels (c) and (g) include both time-even and time-odd polarization effects. Finally, panels (d) and (h) show two variants of the calculations with spin fields readjusted to match empirical Landau parameters, namely the SkO$_{T'L_S}$ (open diamonds) and the SkO$_{T'L_B}$ (filled diamonds) functionals.

resulting from (local) fits to the SO splittings and the SPE [10,46] preferring strong tensor and weak SO terms, on one hand, and large-scale fits to the binding energies [16] pointing toward weak tensor and stronger SO terms, on the other hand. Indeed, the current results indicate that, for large-scale fits, one should explore functionals that have nonstandard forms, including, in particular, functionals with a nonconventional isovector spin-orbit, which characterizes the SkO functional.

V. TIME-EVEN AND TIME-ODD POLARIZATION EFFECTS IN THE PRESENCE OF STRONG TENSOR FIELDS

The aim of this section is to analyze the polarization phenomena that occur in the presence of strong tensor fields and to show that, in spite of the relatively large readjustments as compared to the SkO$_T$ parametrization, the SkO$_{T'}$ functional can still reproduce the empirical $1f_{5/2}$ and $1f_{7/2}$ SO splittings quite well. Figure 5 illustrates the neutron (left-hand side) and proton (right-hand side) SO splittings between the $1f_{5/2}$ and $1f_{7/2}$ SO partners in ^{40}Ca, ^{48}Ca, and ^{56}Ni. The empirical data are indicated by filled circles. The values shown are average means of empirical results taken from Refs. [52] and [53] (see also Table III in Ref. [10] for a compilation of the empirical SO splitting data). Error bars represent deviations from the mean values.

Open circles illustrate the results of our calculations using the original SkO parametrization. Open and filled diamonds represent calculations using the SkO$_{T'}$ functional. In all variants of the calculations, the $C_t^{\Delta s}$ strength was set to zero to ensure convergence. Different panels represent different variants of the calculations that concern treatment of the time-odd sector. Figures 5(a) and 5(e) show bare, unpolarized SO splittings deduced directly from the SP spectra calculated in the doubly magic ^{40}Ca, ^{48}Ca, and ^{56}Ni nuclei. Results presented in the other panels are calculated from the binding energies in the doubly magic cores and their one-particle(hole) odd-A neighbors following the prescription given in Ref. [10]. In the calculations, the odd-A binding energies correspond to fully aligned $\langle I_y \rangle = j$ states at oblate (for one particle) and prolate (for one hole) nuclei, respectively. Unlike in our previous study [10], the current calculations include polarization effects exerted by the odd particle or hole on the even-even core in the presence of strong attractive tensor fields.

To visualize the role of the tensor interaction, particularly in the time-odd sector, we performed three different variants of the calculations. Figures 5(b) and 5(f) include only the time-even (mass and deformation) polarization effect. These results were obtained by setting all time-odd coupling constants to zero. Figures 5(c) and 5(g) illustrate the effect of the time-odd fields. These results include both the time-even and time-odd polarizations. In these calculations, a gauge-invariant functional with the $C_t^T = -C_t^J$ tensor coupling constants fitted to the SO splittings was used. All other coupling constants in this run, except $C_t^{\Delta s} \equiv 0$, are equal to the values given by the SkO parametrization. Note that the splittings calculated in this way match the empirical data almost perfectly. Note also that the time-odd polarization effects are indeed large, reaching a few hundred keV.

Figures 5(d) and 5(h) show two variants of the calculations with spin fields readjusted to match empirical Landau parameters, namely the SkO$_{T'L_S}$ and SkO$_{T'L_B}$ variants (see Sec. II). The SkO$_{T'L_S}$ variant is indicated with open diamonds.

It corresponds to a fully gauge-invariant functional. In this variant we use the $C_t^T = -C_t^J$ tensor coupling constants fitted to the SO splittings and the spin-field coupling constants readjusted to the s-wave Landau parameters according to Eqs. (18) and (19).

In the $\mathrm{SkO}_{T'L_B}$ variant, which is indicated in the figure by filled diamonds, the C_t^T coupling constants are fist readjusted to the Gogny values of the p-wave Landau parameters $g_1 = -0.19$ and $g_1' = 1.2$. This approach leads to a gauge-symmetry-violating functional with the tensorial coupling constant $C_0^J \approx -44.1$ MeV fm^5 and $C_1^J \approx -91.6$ MeV fm^5 in the time-even channel and $C_0^T \approx 9.2$ MeV fm^5 and $C_1^T \approx -29.9$ MeV fm^5 in the time-odd channel, which are used subsequently to calculate spin-field coupling constants. Note that the SO splittings are quite sensitive to the way the functional is set up in the time-odd sector. It means that the entire concept of fitting the time-odd coupling constants to the Landau parameters in the presence of strong tensor terms must be reconsidered. In particular, the p-wave parameters deduced from the Gogny force $g_1 = -0.19$ and $g_1' = 1.2$ lead to C_t^T coupling constants that are completely inconsistent with the time-even values for C_t^J deduced from the SO splittings. In turn, the $\mathrm{SkO}_{T'L_S}$ and $\mathrm{SkO}_{T'L_B}$ variants have entirely different spin fields with coupling constants $C_0^s \approx 426.4$ MeV fm^5 and $C_1^s \approx 48.6$ MeV fm^5 and $C_0^s \approx 18.0$ MeV fm^5 and $C_1^s \approx 155.9$ MeV fm^5, respectively.

VI. EFFECT OF TENSOR FIELD ON NUCLEAR DEFORMATION

In the previous section it was shown that one can construct an EDF capable of reproducing reasonably well the binding energies of the spherical doubly magic nuclei, simultaneously accounting for the SO splittings of the $1f_{7/2}$-$1f_{5/2}$ SP levels. From closer inspection of the results presented in Fig. 2, one observes very strong time-even (mass and deformation) polarization effect on the calculated SO splitting in ^{56}Ni. (Compare Figs. 2(a) and 2(b) or Figs. 2(e) and 2(f). The effect is definitely stronger for the $\mathrm{SkO}_{T'}$ variant than for SkO, indicating that the reduction of the spin-orbit combined with strong attractive tensor fields can affect deformation properties, which are rather well captured by conventional Skyrme forces. Hence, nuclear deformability in the presence of strong attractive tensor fields and reduced SO potential poses a very stringent test for this new class of functionals.

The aim of this section is to show that deformation properties indeed depend sensitively on the balance between the SO and tensor fields. Two contrasting cases are discussed. The first is an example of the yrast superdeformed (SD) band in ^{56}Ni [54]. The band is formed by promoting two protons and two neutrons from the $1f_{7/2}$ to the $1f_{5/2}$ orbital or, in terms more appropriate from an MF point of view in asymptotic Nilsson model quantum numbers, from the [303]7/2 to the [321]3/2 Nilsson orbital, as illustrated schematically in Fig. 6(a).

In the spherical ground state (GS) of ^{56}Ni, the entire $1f_{7/2}$ orbital is fully occupied while the $1f_{5/2}$ orbital is empty. This creates large spin-asymmetry and, in turn, a large contribution

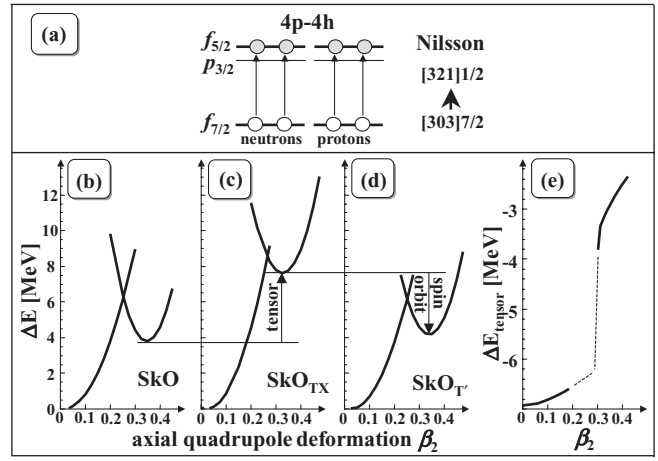

FIG. 6. (a) Schematic of the mechanism underlying the formation of the SD band in ^{56}Ni. It is associated with 4p-4h isoscalar excitation from the $1f_{7/2}$ to the $1f_{5/2}$ orbital. Panels (b)–(d) show potential energy curves for the ground-state and the superdeformed (SD) bands calculated using the SkO, SkO_{TX}, and $\mathrm{SkO}_{T'}$ functionals, respectively. Panels (b) and (c) demonstrate the effect of a strong attractive isoscalar tensor field and panel (d) the effect of reduced spin-orbit field on the excitation energy of the SD band. Panel (e) shows the change in the tensor energy associated with the 4p-4h excitation leading to the SD band.

to the GS from the tensor field. By promoting four-particles from the $1f_{7/2}$ to the $1f_{5/2}$ orbital, one creates the SD state, which has reduced spin-asymmetry compared to the GS. The reduced tensor field shifts the SD state up in energy with respect to the GS. The subsequent reduction of the SO potential shifts the $1f_{5/2}$ orbital and, in turn, the entire SD band down in energy. This compensating mechanism is illustrated in Figs. 6(b)–6(d). The figures show the results of the self-consistent quadrupole-constrained HF calculations for the GS and SD configurations. Because it is impossible to go diabatically through the GS–SD configuration crossing region, the self-consistent results for the GS and SD configurations are, for the sake of simplicity and clarity, extrapolated diabatically through this region. This does not affect the physics discussed later.

Figure 6(b) shows the calculations performed using the conventional SkO force. These calculations predict the 0^+ SD state to be excited by ∼4 MeV with respect to the GS, which agrees quite well with the empirical estimate [54]. Readjustment of the tensor coupling constant in the SkO force to the value characteristic of the $\mathrm{SkO}_{T'}$ functional (this functional is called SkO_{TX}) shifts the position of the 0^+ SD state up in energy by 4 MeV. This intermediate step is illustrated in Fig. 6(c). The change in the tensor field on the passage from the GS to the SD minimum is shown in Fig. 6(e). Finally, Fig. 6(d) shows the result obtained using the full $\mathrm{SkO}_{T'}$ functional. The effects of the reduced SO and strong attractive tensor fields almost cancel each other, restoring the position of the 0^+ SD state close to its empirical (and to the SkO) value.

The second example is shown in Fig. 7. The figure illustrates potential energy curves in ^{80}Zr calculated using the HFB model with volume-δ interaction, $V\delta(\boldsymbol{r})$, of the strength

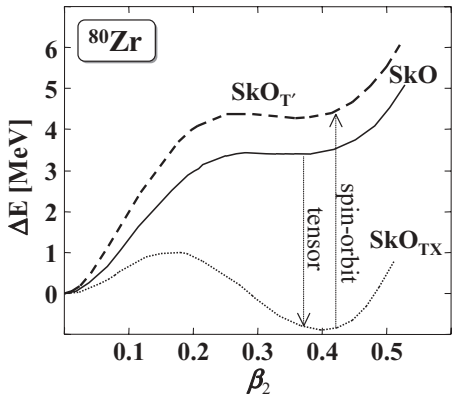

FIG. 7. Potential energy curves calculated using a quadrupole-constrained Skyrme HFB model. The solid curve represents the SkO calculations. Dotted and dashed curves illustrate the SkO_{TX} and $\mathrm{SkO}_{T'}$ results, respectively. Note that the tensor field tends to favor strongly elongated shapes, which leads to a well-deformed absolute minimum. The subsequent reduction of the SO strength, however, shifts the entire potential energy curve up in energy close to its original SkO position.

$V = -190$ MeV in the particle-particle channel. The three curves represent the SkO, SkO_{TX}, and $\mathrm{SkO}_{T'}$ functionals in the particle-hole channel. All curves are normalized to the spherical minimum to facilitate further discussion.

Unlike ^{56}Ni, ^{80}Zr is spin-saturated in the spherical minimum. A deformation buildup is associated in this nucleus with partial occupation of the $1g_{9/2}$ subshell. It leads to increasing spin-asymmetry and, in turn, to extra attraction because of the tensor terms. This effect is clearly visible for the SkO_{TX} functional (see Fig. 7). The mechanism is strong enough to create a well-deformed minimum. In this case, reduction of the SO strength shifts the $1g_{9/2}$ subshell up with respect to the negative-parity fp levels. In turn, the well-deformed minimum is also lifted up in energy and ends up slightly higher than the SkO prediction.

These two examples show that the $\mathrm{SkO}_{T'}$ functional has deformation properties quite similar to those of the conventional Skyrme functionals, at least in isoscalar $N \approx Z$ nuclei. The situation is slightly more intricate in the isovector channel because of the uncertainties of the $C_1^{\nabla J}$ strength and, in turn, in the C_1^J coupling constant. Nevertheless, the two cases analyzed above clearly show that

(i) nuclear deformation properties strongly depend on the balance between tensor and spin-orbit terms;
(ii) detailed and systematic studies of nuclear deformation in the presence of strong tensor fields open up new, promising venues that may help to tune the effective tensor coupling constants C_t^J;
(iii) there is a large, and so far completely unexplored, potential to modify deformation properties by extending the tensor term from the uniform form used here to the nonuniform form (15); and
(iv) possible modifications of collective rotational motion, which is inherently related to the spontaneous breaking of spherical symmetry within the EDF formalism, opens up yet another almost completely unexplored area in studying tensor fields.

VII. SUMMARY AND CONCLUSIONS

The direct fit of the isoscalar spin-orbit and both isoscalar and isovector tensor coupling constants to the $f_{5/2}$-$f_{7/2}$ SO splittings in ^{40}Ca, ^{56}Ni, and ^{48}Ca requires (i) a drastic reduction of the isoscalar SO strength and (ii) strong attractive tensor coupling constants [10]. In this work, the global nuclear structure consequences of this novel fitting strategy of the nuclear EDF were addressed. Among others, we show that the contribution to the nuclear binding energy from the tensor field shows a generic magic structure with the tensorial magic numbers at $N(Z) = 14$, 32, 56, or 90 corresponding to the maximum spin-asymmetries in $1d_{5/2}$, $1f_{7/2} \oplus 2p_{3/2}$, $1g_{9/2} \oplus 2d_{5/2}$, and $1h_{11/2} \oplus 2f_{7/2}$ SP configurations and that these numbers are smeared out by pairing correlations and deformation effects.

We explicitly construct a functional, dubbed $\mathrm{SkO}_{T'}$, which is able to reproduce simultaneously the $f_{5/2}$-$f_{7/2}$ SO splittings in ^{40}Ca, ^{56}Ni, and ^{48}Ca nuclei and the binding energies of spherical nuclei. In fact, one can construct many parametrizations that reproduce these data in a more or less equivalent manner because multidimensional merit functions, which are minimized in the fitting process, are flat in certain directions and the entire minimization procedure is not well defined. Reasonable performance of the binding energies of the $\mathrm{SkO}_{T'}$ functional, which is characterized by its nonconventional isovector SO term, is very interesting by itself. Indeed, this result may open up the possibility of bridging the C^J and $C^{\nabla J}$ coupling constants resulting from (local) fits to the SPE with the values resulting from global large-scale fits to the binding energies by exploring nonstandard local functionals.

Using the $\mathrm{SkO}_{T'}$ functional, polarization effects exerted by one particle and one hole on the values of the $f_{5/2}$-$f_{7/2}$ SO splittings were analyzed. It was shown that the polarization effects are large and very sensitive to the way the functional is set up in the time-odd channel. Fits to the Landau parameters are uncertain due to rather poorly known p-wave Landau parameters. In particular, the use of the p-wave Landau parameters deduced from the Gogny force, which is advocated in Ref. [23], leads to strong gauge-symmetry-violating effects and, in turn, large differences in the C^s coupling constants between the gauge-invariant $\mathrm{SkO}_{T'L_S}$ functional and the gauge-symmetry-violating functional $\mathrm{SkO}_{T'L_B}$.

Deformation properties in atomic nuclei can be easily and strongly modified in the presence of strong tensor fields and these properties are extremely sensitive to the balance between the tensor and the SO coupling constants. For the particular case of the $\mathrm{SkO}_{T'}$ functional, it was shown that the tensor effects are almost perfectly compensated, at least in the isoscalar channel, by the reduced SO potential. We suggest that the role of the tensor interaction, in particular in the time-odd channel, can be studied via dynamic effects induced by fast nuclear rotation. For this purpose one must select and use nuclear states that represent, as closely as possible, an

unperturbed SP motion to suppress other effects or correlations that may obscure the analysis. The examples include SD bands, which have been very well described using a simple one-body cranking approximation (see Ref. [55] and references therein) or terminating states [20].

ACKNOWLEDGMENTS

This work was supported in part by the Polish Ministry of Science under Contracts No. N N202 328234 and No. N N202 239137, by the Göran Gustafsson Foundation, and by the Swedish Science Research Council (VR).

[1] P. Hohenberg and W. Kohn, Phys. Rev. **136**, B864 (1964); M. Levy, Proc. Natl. Acad. Sci. USA **76**, 6062 (1979).
[2] W. Kohn and L. J. Sham, Phys. Rev. **140**, A1133 (1965).
[3] A. Bulgac, Phys. Rev. A **76**, 040502(R) (2007).
[4] P. Klüpfel, P.-G. Reinhard, T. J. Burvenich, and J. A. Maruhn, Phys. Rev. C **79**, 034310 (2009).
[5] D. Gogny, Nucl. Phys. **A237**, 399 (1975).
[6] T. H. R. Skyrme, Philos. Mag. **1**, 1043 (1956); Nucl. Phys. **9**, 615 (1959).
[7] I. Hamamoto, Phys. Lett. **B61**, 343 (1976).
[8] V. Bernard and N. Van Giai, Nucl. Phys. **A348**, 75 (1980).
[9] E. Litvinova and P. Ring, Phys. Rev. C **73**, 044328 (2006).
[10] M. Zalewski, J. Dobaczewski, W. Satuła, and T. R. Werner, Phys. Rev. C **77**, 024316 (2008).
[11] M. Zalewski, W. Satuła, J. Dobaczewski, P. Olbratowski, M. Rafalski, T. R. Werner, and R. A. Wyss, Eur. Phys. J. A **42**, 577 (2009).
[12] W. Satuła, M. Zalewski, J. Dobaczewski, P. Olbratowski, M. Rafalski, T. R. Werner, and R. A. Wyss, Int. J. Mod. Phys. E **18**, 808 (2009).
[13] Y. M. Engel, D. M. Brink, K. Goeke, S. J. Krieger, and D. Vautherin, Nucl. Phys. **A249**, 215 (1975).
[14] M. Bender, P.-H. Heenen, and P.-G. Reinhard, Rev. Mod. Phys. **75**, 121 (2003).
[15] E. Perlińska, S. G. Rohoziński, J. Dobaczewski, and W. Nazarewicz, Phys. Rev. C **69**, 014316 (2004).
[16] T. Lesinski, M. Bender, K. Bennaceur, T. Duguet, and J. Meyer, Phys. Rev. C **76**, 014312 (2007).
[17] J. Dobaczewski, H. Flocard, and J. Treiner, Nucl. Phys. **A422**, 103 (1984).
[18] E. Chabanat, P. Bonche, P. Haensel, J. Meyer, and R. Schaeffer, Nucl. Phys. **A627**, 710 (1997); **A635**, 231 (1998).
[19] P.-G. Reinhard, D. J. Dean, W. Nazarewicz, J. Dobaczewski, J. A. Maruhn, and M. R. Strayer, Phys. Rev. C **60**, 014316 (1999).
[20] W. Satuła, R. A. Wyss, and M. Zalewski, Phys. Rev. C **78**, 011302(R) (2008).
[21] A. N. Ostrowski *et al.*, Z. Phys. A **343**, 489 (1992).
[22] M. Bender, J. Dobaczewski, J. Engel, and W. Nazarewicz, Phys. Rev. C **65**, 054322 (2002).
[23] H. Zduńczuk, W. Satuła, and R. A. Wyss, Phys. Rev. C **71**, 024305 (2005); Int. J. Mod. Phys. E **14**, 451 (2005).
[24] E. Becheva *et al.*, Phys. Rev. Lett. **96**, 012501 (2006).
[25] M. Belleguic *et al.*, Phys. Rev. C **72**, 054316 (2005).
[26] Y. Utsuno, T. Otsuka, T. Glasmacher, T. Mizusaki, and M. Honma, Phys. Rev. C **70**, 044307 (2004).
[27] V. Tripathi *et al.*, Phys. Rev. Lett. **94**, 162501 (2005).
[28] G. Neyens *et al.*, Phys. Rev. Lett. **94**, 022501 (2005).
[29] B. Fornal *et al.*, Phys. Rev. C **70**, 064304 (2004).
[30] D.-C. Dinca, R. V. F. Janssens, A. Gade, D. Bazin, R. Broda, B. A. Brown, C. M. Campbell, M. P. Carpenter, P. Chowdhury, J. M. Cook, A. N. Deacon, B. Fornal, S. J. Freeman, T. Glasmacher, M. Honma, F. G. Kondev, J. L. Lecouey, S. N. Liddick, P. F. Mantica, W. F. Mueller, H. Olliver, T. Otsuka, J. R. Terry, B. A. Tomlin, and K. Yoneda, Phys. Rev. C **71**, 041302 (2005).
[31] T. Otsuka, R. Fujimoto, Y. Utsuno, B. A. Brown, M. Honma, and T. Mizusaki, Phys. Rev. Lett. **87**, 082502 (2001).
[32] T. Otsuka, T. Suzuki, R. Fujimoto, H. Grawe, and Y. Akaishi, Phys. Rev. Lett. **95**, 232502 (2005).
[33] M. Honma, T. Otsuka, B. A. Brown, and T. Mizusaki, Eur. Phys. J. A **25**, s01, 499 (2005).
[34] T. Otsuka, T. Matsuo, and D. Abe, Phys. Rev. Lett. **97**, 162501 (2006).
[35] M. Sawicka *et al.*, Eur. Phys. J. A **20**, 109 (2003).
[36] A. Korgul (private communication).
[37] J. P. Schiffer *et al.*, Phys. Rev. Lett. **92**, 162501 (2004).
[38] D. Brink, Fl. Stancu, and H. Flocard, Phys. Lett. **B68**, 108 (1977).
[39] B. A. Brown, T. Duguet, T. Otsuka, D. Abe, and T. Suzuki, Phys. Rev. C **74**, 061303(R) (2006).
[40] G. Colò, H. Sagawa, S. Fracasso, and P. F. Bortignon, Phys. Lett. **B646**, 227 (2007).
[41] D. M. Brink and F. Stancu, Phys. Rev. C **75**, 064311 (2007).
[42] M. Beiner, H. Flocard, N. Van Giai, and P. Quentin, Nucl. Phys. **A238**, 29 (1975).
[43] J. Bartel, P. Quentin, M. Brack, C. Guet, and H. B. Håkansson, Nucl. Phys. **A386**, 79 (1982).
[44] B. A. Brown, Phys. Rev. C **58**, 220 (1998).
[45] K. Bennaceur and J. Dobaczewski, Comput. Phys. Commun. **168**, 96 (2005).
[46] M. Kortelainen, J. Dobaczewski, K. Mizuyama, and J. Toivanen, Phys. Rev. C **77**, 064307 (2008).
[47] J. Dobaczewski, J. Dudek, and P. Olbratowski, Comput. Phys. Commun. **158**, 158 (2004); HFODD User's Guide nucl-th/0501008.
[48] G. Audi, A. H. Wapstra, and C. Thibault, Nucl. Phys. **A729**, 337 (2003); G. Audi and A. H. Wapstra, *ibid.* **A565**, 1 (1993).
[49] T. Baumann *et al.*, Nature **449**, 1022 (2007).
[50] P.-H. Heenen, Nature **449**, 992 (2007).
[51] W. Nazarewicz and M. Stoitsov (private communication).
[52] A. Oros, Ph.D. thesis, University of Köln, 1996.
[53] N. Schwierz, I. Wiedenhover, and A. Volya, arXiv:0709.3525.
[54] D. Rudolph *et al.*, Phys. Rev. Lett. **82**, 3763 (1999).
[55] W. Satuła and R. Wyss, Rep. Prog. Phys. **68**, 131 (2005).